THE JOURNAL OF PHYSICAL CHEMISTRY B

Article

pubs.acs.org/JPCB

The Role of the Crystallization Temperature on the Nanophase Structure Evolution of Poly[(*R*)-3-hydroxybutyrate]

Maria Cristina Righetti,*[,†] Elpidio Tombari,[†] and Maria Laura Di Lorenzo[‡]

[†]Consiglio Nazionale delle Ricerche − Istituto per i Processi Chimico-Fisici, INSTM, UdR Pisa, Via G. Moruzzi 1, 56124 Pisa, Italy

[‡]Consiglio Nazionale delle Ricerche − Istituto di Chimica e Tecnologia dei Polimeri, c/o Comprensorio Olivetti, Via Campi Flegrei 34, 80078 Pozzuoli (NA), Italy

ABSTRACT: The nanophase structure of semicrystalline polymers, which determines the mechanical, thermal, and gas permeability behavior, can be quantified by thermal methods. A detailed investigation of the nanophase structure of poly[(R)-3-hydroxybutyrate] (PHB) was performed under conditions of isothermal, quasi-isothermal, and nonisothermal crystallizations. The experimental analyses revealed that the establishment of the nanophase rigid amorphous fraction (RAF) in PHB depends on the temperature at which crystallization occurs. The RAF grows in parallel with the crystal phase during quasi-isothermal crystallization at 30 °C, whereas during nonisothermal crystallization at higher temperatures, RAF starts to develop at 70 °C, in correspondence with the final stages of the crystallization process. The influence of crystallization temperature on the nanophase structure was rationalized taking into account the effect of the mobility of the entangled chain segments during the phase transition. The melting behavior was found to change after isothermal crystallization at 70 °C, revealing that complete RAF mobilization is achieved approximately at this temperature. The temperature of 70 °C could be the limit for the formation and the disappearance of rigid amorphous fraction in the PHB analyzed in the present study.

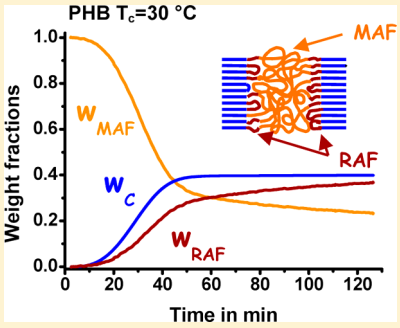

INTRODUCTION

The structure of semicrystalline polymers is determined by competition between crystallization and vitrification and is established during material processing. The common description of semicrystalline polymers as constituted by two separate phases, one amorphous and one crystalline, has been recently replaced by a more complete one that also takes into account the intermediate nanophase present at the interface between the crystals and the surrounding melt.[1] The decoupling between crystalline and amorphous phases is in general incomplete, due to the length of the polymer molecules, which are much higher than the dimensions of the crystalline phase, at least in one direction, and to possible geometrical constraints that can be established during crystallization. The interphase is noncrystalline and includes amorphous chain portions whose mobility is hindered by the near crystalline structures. This interphase is generally named "rigid amorphous fraction" (RAF), its mobility being lower than that of the unconstrained amorphous phase, which is usually addressed as "mobile amorphous fraction" (MAF).

The temperature at which the rigid amorphous fraction vitrifies or mobilizes is often located between the glass transition (T_g) of the unstrained amorphous phase and the melting temperature, but this is not a general rule. In some polymers, the presence of RAF may cause a separate glass transition,[1] but more often the exact location of the RAF vitrification and devitrification cannot be directly identified by DSC analysis, because these processes are associated with the continuous and progressive change of the structure between solid and liquid and vice versa that occurs during a cooling or a heating scan. In fact, due to the various degrees of coupling that the noncrystallized chain portions may have with the crystal phase, RAF vitrification and devitrification generally take place in a very wide temperature range, which often overlaps crystal ordering or disordering.[2]

The relationship between crystal growth and rigid amorphous fraction development has been detailed in the literature only for a limited number of semicrystalline polymers.[3−10] During crystallization of poly(ethylene terephthalate) (PET) and poly[(*R*)-3-hydroxybutyrate] (PHB) at temperatures slightly above the respective T_g's, vitrification of the rigid amorphous fraction parallels crystal growth,[3,10] whereas in isotactic polystyrene (iPS) crystallized at 140 and 170 °C, i.e., well above the bulk T_g, the rigid amorphous fraction increases markedly after spherulite impingement, which corresponds to the beginning of the crystallization in restricted regions.[4,5] Upon slow cooling from the melt, both in iPS and PET, RAF vitrification takes place during the final stages of the nonisothermal crystallization process, with the full establishment of the rigid amorphous structure completed during the subsequent cooling to room temperature.[6,7] Conversely, a much slower cooling rate from the melt, attained with quasi-isothermal step cooling, results in vitrification of the RAF in PET only after completion of crystallization.[8] All these analyses,

Received: June 26, 2013
Revised: September 10, 2013
Published: September 10, 2013

dx.doi.org/10.1021/jp4063127 | *J. Phys. Chem. B* 2013, 117, 12303−12311

conducted independently of one another, in different crystallization conditions and with different methods of data processing, prove that the thermal history of the samples can affect the combined evolution of the different solid phases. The influence of the crystallization temperature was specifically investigated for poly(L-lactic acid) (PLLA): in PLLA, RAF develops in parallel to the crystal phase at low crystallization temperatures, whereas at high T_c, the rigid amorphous fraction is established only during the final stages of crystallization, in correspondence with the growth of secondary crystals.[11]

Also the melting process was found to be partially linked to RAF mobilization for a number of different semicrystalline polymers that display a multiple melting behavior.[4,5,9−16] For bisphenol A polycarbonate, RAF devitrification occurs simultaneously with the melting of thinner and more defective crystals, in correspondence with the low-temperature endotherm located a few degrees above the temperature of isothermal crystallization.[9,10] For PET and iPS, the low-temperature endotherm was probed to be connected with both partial fusion of the crystalline portions and enthalpy recovery subsequent to structural relaxation of the rigid amorphous fraction.[4,5,13] For *cis*-1,4-polybutadiene, which can display up to three major melting peaks, it was even demonstrated that not only the first endotherm, but also the overall multiple fusion behavior is affected by the physical state of the RAF, since it is only in the temperature range of the second major endotherm that the rigid amorphous fraction attains sufficient mobility to allow development of perfected crystals with higher melting point.[14] On the contrary, for poly(1-butene), RAF devitrification is completed well below the melting region.[17,18]

On the basis of these results, it would be of enormous interest to clarify how the thermal history controls the kinetics of the RAF development, and rationalize the link between crystal growth and RAF vitrification. In addition, it would also be important to identify the connection between the conditions of development and of disappearance upon heating of the rigid amorphous fraction. These data are essential for a deeper understanding of the structure−property−processing triangle of semicrystalline polymers, since the nanophase structure determines the material behavior, including thermal, barrier, and mechanical properties.[17,19−23] As a matter of fact, by acting as a stress transfer point, RAF produces an increase in the elastic modulus, with a behavior similar to that of the crystal phase,[17,19,22] whereas, as regards gas permeability, RAF is more permeable for small molecules because of its high free volume.[20,21,23]

In order to verify the possible existence of a general rule for the development and the disappearance of the rigid amorphous fraction, the crystallization and melting processes of poly[(*R*)-3-hydroxybutyrate)] were studied and analyzed by conventional and temperature modulated differential scanning calorimetry.

PHB is a naturally occurring polyester that constitutes an important storage material in a wide variety of bacteria which, when grown in particular conditions, are able to accumulate PHB in the storage phase up to 70% of the total dry mass.[24] In the last decades, the properties of microbial PHB have been deeply investigated for both technological and scientific reasons. PHB is a rare example of hydrophobic polymer fully biodegradable and biocompatible, with relatively high melting point and crystallinity.[25] These properties make PHB a useful thermoplastic material for utilization in biomedical fields and for low environmental impact applications. For the purpose of this study, PHB is an interesting polymer because it does not evidence consistent reversing melting when subjected to temperature modulation, at least at temperatures close to T_g.[10]

The rigid amorphous fraction of PHB at T_g was reported to be around 10−20% of the overall sample mass,[10,26−29] somewhat higher values were also determined for oligomeric PHB.[30,31] In an our recent study, the effect of RAF on the crystallization mechanism was analyzed.[32] During heating of an initially amorphous PHB, RAF, which is established simultaneously with the crystal formation during the first stage of cold crystallization, slows down further crystal growth, which can proceed further only at temperatures higher than 70 °C, when complete mobilization of the RAF is achieved.[32]

In another recent publication, we demonstrated that in PHB, the kinetics of vitrification of the amorphous regions is affected by the thermal history of the material.[27] Slow cooling from the melt results in crystallization at high temperatures and a low RAF content. Higher cooling rates from the melt reduce the crystalline fraction at room temperature, which results in a higher vitrification of the RAF during the storage at 25 °C.[27] Now we have expanded this study, with the aim to clarify the vitrification and devitrification range of PHB in relation to the crystallization temperature.

EXPERIMENTAL METHODS

Poly[(*R*)-3-hydroxybutyrate] with molar mass 435 000 g mol^{-1} was purchased from Aldrich Chemical Co., Inc. The polymer had the consistency of a fine powder and was used as received without further purification or thermal treatment.

Differential scanning calorimetry (DSC) and temperature-modulated calorimetry (TMDSC) measurements were performed with a Perkin-Elmer Differential Scanning Calorimeter DSC 8500 equipped with an IntraCooler III as refrigerating system. The instrument was calibrated in temperature with high purity standards (indium, naphthalene, cyclohexane) according to the procedure for standard DSC.[33] Energy calibration was performed with indium. In order to gain precise heat capacity data from the heat flow rate measurements, each scan was accompanied by an empty pan run and calibration with sapphire.[33]

Dry nitrogen was used as purge gas at a rate of 30 mL min^{-1}. A fresh sample was employed for each analysis in order to minimize thermal degradation. All the results presented and discussed are the average of three repeated runs. Before the analyses, each PHB sample was heated to 193 °C at a rate of 50 °C min^{-1} and maintained at this temperature for 3°min.[34] These are the optimized experimental conditions that allow the complete fusion of previous crystal order, and at the same time ensure the minimum possible thermal degradation of PHB chains.[35]

After cooling the samples from 193 to 140 °C by ballistic cooling (cooling time = 0.25 min), nonisothermal crystallization of PHB was followed both by TMDSC and conventional DSC down to −40 °C at −2 °C min^{-1}. Modulated and conventional DSC heating runs up to 200 °C at +2 °C min^{-1} were performed immediately after the modulated and linear cooling scans respectively. TMDSC analyses were designed using a sawtooth modulation temperature program. Measurements were conducted with a temperature amplitude (A_T) of 1.0 °C and modulation periods (p) of 60 and 120 s. For p = 60 s, the semiperiod rates on cooling were −6.0 °C min^{-1} and +2.0 °C min^{-1}, and the semiperiod rates on heating were +6.0 °C min^{-1} and −2.0 °C min^{-1}. For p = 120 s, temperature modulation was obtained on cooling with

dx.doi.org/10.1021/jp4063127 | J. Phys. Chem. B 2013, 117, 12303−12311

a cooling step of 1 min at −4 °C min^{-1} followed by an isothermal step of 1 min, and on heating with a heating step of 1 min at +4 °C min^{-1} followed by an isothermal step of 1 min.

Quasi-isothermal TMDSC crystallization was conducted at 30 °C after fusion of the samples at 193 °C for 3 min and ballistic cooling (cooling time from 193 to 30°C = 1.3 min). The temperature program involved a modulation amplitude of 1.0 °C and periods of 60 and 120 s, respectively. For p = 60 s, the semiperiod rates were −4.0 °C min^{-1} and +4.0 °C min^{-1}, for p = 120 s the semiperiod rates were −2.0 °C min^{-1} and +2.0 °C min^{-1}. At the end of crystallization, the samples were cooled down to −40 °C with ballistic cooling (cooling time = 1.3 min) and reheated at 10 °C min^{-1} up to 200 °C by conventional DSC.

According to the mathematical treatment of TMDSC data, the modulated temperature and the heat flow rate curves can be approximated to Fourier series.[36−39] From the ratio between the amplitudes of the first harmonic of the heat flow rate and temperature, the reversing specific heat capacity ($c_{p,rev}$) is obtained:

$$c_{p,rev}(\omega, t) = \frac{A_{HF}(t)}{A_T(t)} \frac{K(\omega, t)}{m\omega} \quad (1)$$

where ω is the frequency of temperature modulation ($\omega = 2\pi/p$), t the time, $A_{HF}(t)$ and $A_T(t)$ the amplitudes of the first harmonic of the heat flow rate and temperature modulation respectively, and m the mass of the sample. The frequency-dependent calibration factor, $K(\omega,t)$, determined by calibration with sapphire, was 1.05 and 1.00 for p = 60 and 120 s, respectively. The correctness of the calibration factor was proven by the good agreement between the PHB measured solid and liquid specific heat capacities and the literature solid and liquid c_p data,[9] as reported below.

Isothermal crystallizations of PHB were conducted at various crystallization temperatures (40 °C ≤ T_c ≤ 110 °C) for 40 min, after fusion of the samples at 193 °C and ballistic cooling down to T_c. At the end of crystallization, the samples were reheated at 5 °C min^{-1} and 10 °C min^{-1} directly from T_c up to 200 °C by conventional DSC.

RESULTS AND DISCUSSION

Nonisothermal TMDSC Crystallization and Successive Melting. Figure 1A shows the specific heat capacity (c_p) of PHB from conventional DSC together with the corresponding reversing specific heat capacity ($c_{p,rev}$) from TMDSC with p = 60 and 120 s, during cooling and the successive heating at −2 °C min^{-1} and +2 °C min^{-1} respectively. On the same graph, the specific heat capacity data in the liquid and solid state of PHB, as taken from the literature, are also indicated.[9] An enlargement of the plots is presented in Figure 1B to show details of the $c_{p,rev}$ curves. It is worth noting that the specific heat capacity is positive for both crystallization and melting, since for the former process the enthalpy decreases as the average temperature decreases, whereas for the latter process the enthalpy increases with the average temperature. The c_p curves depicted in Figure 1 reveal that the crystallization process extends from about 130 °C down to approximately 40 °C, with the peak centered at 108.5 °C, whereas the fusion, which ends approximately at 182 °C, presents a peak at 175.5 °C and a shoulder on the high temperature side of the endotherm. The glass transition, related to the vitrification/

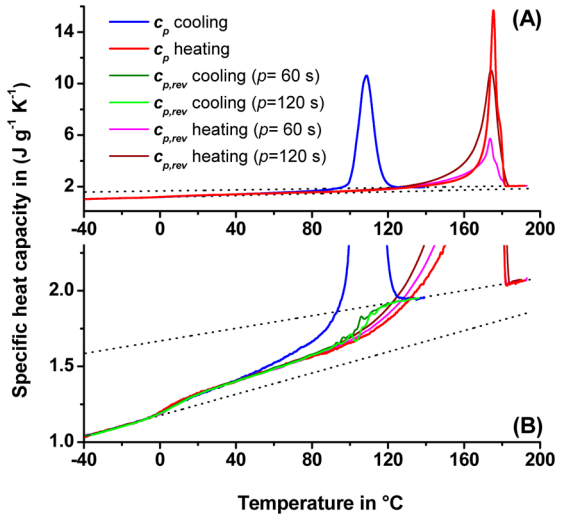

Figure 1. (A) Specific heat capacity (c_p) and reversing specific heat capacity ($c_{p,rev}$) at modulation periods of 60 and 120 s of PHB upon cooling from the melt at −2 °C min^{-1} and successive heating at +2 °C min^{-1}. The black thin dotted lines are the solid and liquid PHB specific heat capacities.[9] Graph B is an enlargement of graph A to show details of the $c_{p,rev}$ curves.

mobilization of the MAF, occurs in the range −10 to 20 °C and is centered at 4.5 °C.

At temperatures below about 70 °C, the perfect correspondence between the $c_{p,rev}$ curves, which are independent of the frequency of modulation and are identical upon both cooling and heating, suggests that no or minor reversing latent heat is exchanged in this temperature range (Figure 1B). As a result, between the glass transition temperature and approximately 70 °C, the $c_{p,rev}$ curves correspond to the baseline heat capacity ($c_{p,base}$), i.e., the specific heat capacity without contributions from latent heat.[10] Also in correspondence with the crystallization peak, the $c_{p,rev}$ curves upon cooling seem frequency independent. The experimental plots overlap and both show a sigmoidal shape, as expected for the crystallization baseline, though some spurious effects are also evident in the range 100−120 °C. This kind of signal noise, generally observed in the presence of sharp transitions, arises from the approximations used in the elaboration of the TMDSC signal,[40] and proves that nonstationary conditions slightly affect the measurement of $c_{p,rev}$ in the PHB crystallization range.[41,42] Nevertheless, the $c_{p,rev}$ curves can be reasonably assumed as a good approximation of $c_{p,base}$ for the cooling step, due to the absence of sizable reversing latent heat exchange. Conversely, the marked frequency dependence of $c_{p,rev}$ above 70 °C upon heating proves the occurrence of thermal processes involving reversing exchanges of latent heat, as typical of polymer melting.[2,10,43] In the temperature range from 70 °C up to about 170 °C, the reorganization of PHB crystals into more stable structures takes place markedly, as attested by the $c_{p,rev}$ values that are higher than the corresponding c_p data. This is due to the method of calculation of the reversing heat capacity (eq 1). The amplitude of modulated heat flow is derived from the sum of the absolute values of the endothermic and exothermic events intensity occurring within each modulation period, whereas the latent heat released or absorbed sum algebraically when the specific heat capacity (c_p) is determined.[13,39] Above 170 °C up to the end of the melting, the $c_{p,rev}$ values are lower than the corresponding c_p data, which probes that the final PHB

dx.doi.org/10.1021/jp4063127 | J. Phys. Chem. B 2013, 117, 12303−12311

melting process is a largely irreversible event, which occurs during both the modulation semiperiods.[13]

From the c_p curves of Figure 1, growth and the disappearance of the crystal fraction were calculated for cooling and heating respectively, by using the classical two-phase enthalpy-based procedure summarized in eq 2,[44] neglecting, as a first approximation, possible vitrification and devitrification of the rigid amorphous fraction:

$$w_{C,2phase}(T) = \frac{\int_{T_o}^{T} [c_p(T') - c_{p,L}(T')]\, dT'}{\Delta h_m^{\circ}(T)} \quad (2)$$

where T_o is a reference temperature in the melt, $c_{p,L}$ the thermodynamic specific heat capacity of the melt and Δh_m° the heat of fusion of the 100% crystalline PHB ($\Delta h_m^{\circ}(T) = 80.44 + 0.492 \cdot T - 0.00071 \cdot T^2$) with T in °C.[32]). The calculated two-phase crystalline fractions for cooling and heating are depicted in Figure 2. Both the $w_{C,2phase}$ curves exhibit a central plateau. At

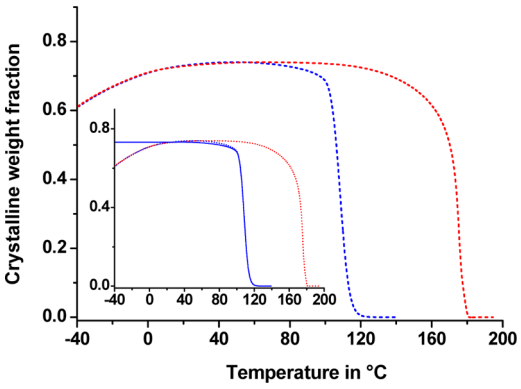

Figure 2. Temperature evolution of the crystalline weight fraction from the two phase method ($w_{C,2phase}$) for PHB cooled at −2 °C min^{-1} and successively heated at +2 °C min^{-1} (blue and red dashed lines respectively). In the inset the temperature evolution of the approximate crystalline weight fraction from the three-phase method ($w_{C,3phase}$) for PHB upon cooling at −2 °C min^{-1} (solid blue line) is also depicted.

temperatures lower than 40 °C, the crystal fraction decreases as the temperature decreases toward the glass transition. Also in the glassy state the calculated crystal weight fraction continues unexpectedly to decrease. As it is impossible that partial fusion takes place on cooling at temperatures lower than 40 °C, it is evident that some errors occur in the data processing. In previous articles it was shown that the discrepancy arises from the vitrification/devitrification of the rigid and mobile amorphous fractions, which are ignored in the calculations based on eq 2.[6,7]

Only assuming a three-phase model, the precise determination of the crystalline fraction in the entire temperature range from below T_g up to fusion can be achieved. The necessary condition for the quantification of the three-phase structure is the knowledge of the $c_{p,base}$ curve, which is defined as

$$c_{p,base}(T) = w_{C,3phase}(T)c_{p,C}(T) + w_{RAF}(T)c_{p,C}(T) + w_{MAF}(T)c_{p,L}(T) \quad (3)$$

where $w_{C,3phase}$, w_{RAF}, and w_{MAF} are the weight fraction of the crystalline, rigid amorphous, and mobile amorphous fraction, respectively, and $c_{p,C}$ and $c_{p,L}$ are the thermodynamic specific heat capacities of the solid and the liquid. The RAF specific heat capacity is assumed equal to that of the crystal phase, both being considered as solid fractions.[44] The baseline specific heat capacity is connected to c_p through the following relationship:[6,44]

$$c_p(T) = c_{p,base}(T) + \Delta h_m^{\circ}(T)\frac{dw_{C,3phase}(T)}{dT} \quad (4)$$

from which the crystalline weight fraction curve $w_{C,3phase}$ can be determined:

$$w_{C,3phase}(T) = \int_{T_o}^{T} \frac{c_p(T') - c_{p,base}(T')}{\Delta h_m^{\circ}(T')}\, dT' \quad (5)$$

where T_o is a reference temperature in the melt. From the baseline specific heat capacity the mobile amorphous weight fraction (w_{MAF}) can be calculated according to following relationship:[6]

$$w_{MAF}(T) = \frac{c_{p,base}(T) - c_{p,C}(T)}{c_{p,L}(T) - c_{p,C}(T)} \quad (6)$$

Finally the rigid amorphous weight fraction w_{RAF} can be obtained by difference, being $w_C + w_{MAF} + w_{RAF} = 1$. If the proper $c_{p,base}$ cannot be attained by means of the TMDSC analysis, as a first step an approximate baseline specific heat capacity can be applied, and the correct $c_{p,base}$ and $w_{C,3phase}$ established through successive approximations, as detailed below.

For the cooling, as a first approximation, the baseline specific heat capacity can be provided by the average of the $c_{p,rev}$ curves. The resulting $w_{C,3phase}$, calculated by eq 5, is presented in the inset of Figure 2. The first feature that hits the eye is the trend of $w_{C,3phase}$ curve, which exhibits a value that remains constant as the temperature lowers toward the glassy state, unlike the two-phase crystalline fraction that displays an unreliable reduction in the same temperature interval.

From $w_{C,2phase}$ and $w_{C,3phase}$, the two-phase approximate baseline heat capacity curves ($c_{p,appr,2}$ and $c_{p,appr,3}$) upon cooling, both neglecting the rigid amorphous fraction vitrification, were calculated via eqs 7 and 8, and compared in Figure 3:

$$c_{p,appr,2}(T) = w_{C,2phase}(T)c_{p,C}(T) + (1 - w_{C,2phase}(T))c_{p,L}(T) \quad (7)$$

$$c_{p,appr,3}(T) = w_{C,3phase}(T)c_{p,C}(T) + (1 - w_{C,3phase,}(T))c_{p,L}(T) \quad (8)$$

Figure 3 shows that the baseline curves derived from eqs 7 and 8 overlap from the beginning of the crystallization down to about 20 °C, where the onset of glass transition of the MAF is located. Their value is slightly lower than that of $c_{p,rev}$ in the temperature range 120−70 °C, because of a 'reversing' effect likely caused by changes in the crystallization rate in the two semiperiods of modulation.[6] Moreover, the $c_{p,appr,2}$ and $c_{p,appr,3}$ lines cross $c_{p,rev}$ at about 70 °C, and at temperatures below 70 °C, their value exceeds the experimental $c_{p,rev}$. Since $c_{p,rev}$ corresponds to the baseline specific heat capacity at temperatures lower than about 70 °C, these results indicate that during nonisothermal crystallization at −2 °C min^{-1}, the rigid amorphous fraction starts to develop at 70 °C. Thus the definitive $c_{p,base}$ curve for the cooling run can be constructed by

dx.doi.org/10.1021/jp4063127 | J. Phys. Chem. B 2013, 117, 12303−12311

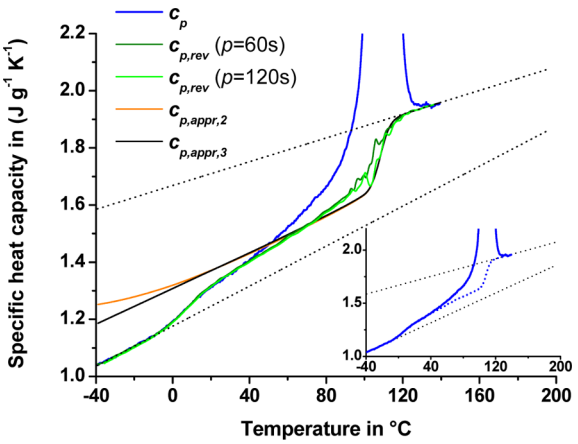

Figure 3. Specific heat capacity (c_p) and reversing specific heat capacity ($c_{p,rev}$) at modulation periods of 60 and 120 s of PHB upon cooling from the melt at −2 °C min^{-1} The black thin dotted lines are the solid and liquid PHB specific heat capacities.[9] The orange line is the $c_{p,appr,2}$ calculated from eq 7, whereas the black solid line is the $c_{p,appr,3}$ calculated from eq 8. In the inset the specific heat capacity (c_p) (blue solid line) together with the final $c_{p,base}$ (dotted blue line) curves are depicted.

merging the $c_{p,appr,2}$ curve from the beginning of the crystallization down to 70 °C, to the $c_{p,rev}$ curve, from 70 °C down to the glassy state (inset of Figure 3). The final $w_{C,3phase}$ from eq 5, together with w_{MAF} from eq 6 and the w_{RAF} obtained by difference, are depicted in Figure 4.

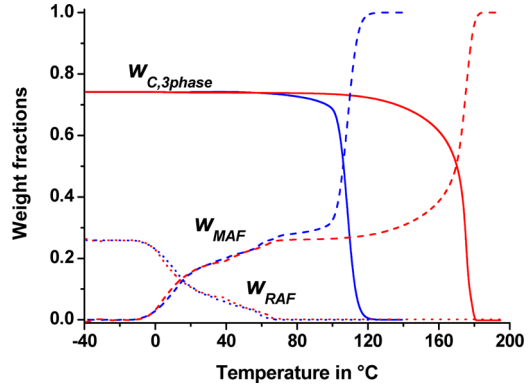

Figure 4. Temperature evolution of crystalline ($w_{C,3phase}$, solid lines), mobile amorphous, (w_{MAF}, dashed lines) and rigid amorphous fraction (w_{RAF}, dotted lines) weight fractions of PHB from the three-phase method upon cooling at −2 °C min^{-1} and successive heating at +2 °C min^{-1} (blue and red lines respectively).

Figure 4 reveals that during nonisothermal crystallization of PHB at −2 °C min^{-1}, RAF starts to develop almost at the end of the crystallization process, during the final stages. At the end of crystallization (about 40 °C), the rigid amorphous fraction is 0.05. However, RAF vitrification occurs also after completion of the crystallization, as evidenced by the w_{RAF} increase occurring in the range 40−20 °C (at 20 °C w_{RAF} = 0.09). Since RAF originates from amorphous segments that are constrained above the bulk T_g, it is likely that internal stresses, which are not released during crystal growth and are concentrated at the amorphous/crystal interface, result in some additional RAF vitrification upon cooling after completion of crystallization, because of the reduced mobility of the chains.[6,7,45]

The crystalline content determined from the three-phase method (eq 5) is 0.74, and corresponds to the maximum crystalline value exhibited by the $w_{C,2phase}$ curve. Such correspondence can be ascribed to the fact that vitrification of the rigid amorphous fraction occurs only at advanced crystallization times.

The three-phase method, as it is constructed and formulated, describes, in addition to crystallization, the evolution of both the amorphous fractions upon cooling. This explains the w_{RAF} trend reproduced in Figure 4: at temperatures lower than 20 °C, the w_{RAF} curve reflects the vitrification of the more mobile amorphous fraction, which ends approximately at −10 °C: below this temperature w_{RAF} is practically constant.

For the calculation of $w_{C,3phase}$ upon heating, as a first approximation the two-phase baseline heat capacity from $w_{C,2phase}$ data was calculated (eq 7). Figure 5 shows that $c_{p,appr,2}$

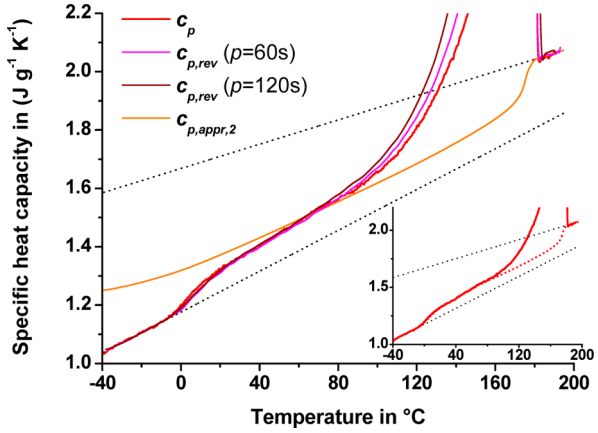

Figure 5. Specific heat capacity (c_p) and reversing specific heat capacity ($c_{p,rev}$) at modulation periods of 60 and 120 s of PHB upon heating at +2 °C min^{-1}. The black thin dotted lines are the solid and liquid PHB specific heat capacities.[9] The orange line is the $c_{p,appr,2}$ calculated from eq 7. In the inset the specific heat capacity (c_p) (red solid line) together with the final $c_{p,base}$ (dotted red line) curves are depicted.

crosses the c_p and the $c_{p,rev}$ curves approximately at 70 °C, which is the superior limit of the temperature range in which $c_{p,base}$ is accessible. As for cooling, the $c_{p,base}$ curve was thus constructed by merging the $c_{p,rev}$ curve, from the glassy state up to 70 °C, to the $c_{p,appr,2}$ curve, from 70 °C to the end of melting (inset of Figure 5). The calculated $w_{C,3phase}$ from eq 5, together with w_{MAF} from eq 6 and w_{RAF}, are illustrated in Figure 4. The perfect correspondence between the $w_{C,3phase}$ values in the glassy state calculated from both the cooling and the heating scans proves the correctness of the heating $c_{p,base}$ curve. The w_{RAF} trends indicate that the RAF mobilization parallels RAF development: upon heating, RAF mobilizes at the same temperature at which it had previously grown during the solidification process. Complete RAF mobilization occurs at about 70 °C, i.e. at the same temperature at which RAF starts to develop on cooling. These results confirm the findings detailed in a previous study, where it was demonstrated that full RAF devitrification of PHB is attained around 70 °C.[32] Thermal analysis of initially amorphous PHB revealed that cold crystallization proceeds via a two-stage process. The rigid amorphous structure, established simultaneously with the crystal growth during the first stage of cold crystallization, slows down the crystallization rate before completion. Only at

dx.doi.org/10.1021/jp4063127 | J. Phys. Chem. B 2013, 117, 12303−12311

temperatures above 70 °C, once the immobilized segments have gained sufficient mobility, can chain rearrangements take place and crystallization proceed further.[32]

From all these observations, the key factor that regulates the RAF formation in PHB appears to be mainly the temperature range where solidification occurs. Temperature is closely related to the mobility of polymer chains: at higher temperatures, the polymer chains have enhanced mobility, which facilitates the organization of the polymeric segments into ordered crystal structures, with reduced stress transmitted to the amorphous segments, and, in turn a lower fraction of chain segments subjected to geometrical constraints. The validity of this hypothesis was recently demonstrated for poly(L-lactic acid), as it was proven that the rigid amorphous fraction grows in parallel with crystalline phase during crystallization at 90 °C, whereas at 130 °C RAF starts to appear approximately in correspondence with secondary crystallization.[11] At $T_c \geq 135$ °C crystal formation proceeds without vitrification of the amorphous segments coupled with the crystals.[11] Also for isotactic polystyrene, different behaviors were evidenced depending on crystallization temperature: during crystallization at 140 and 170 °C, the rigid amorphous fraction was found to develop mostly after spherulite impingement, i.e., in correspondence with crystallization in restricted areas,[4] whereas crystallization conducted nonisothermally at −2 °C min^{-1} and −3 °C min^{-1}, with crystallization peak centered at about 210 °C, evidenced that the beginning of RAF vitrification occurs during the final stages of the process, at times longer than the spherulite impingement event.[7] These findings underline that the thermal history, in particular the rate and temperature at which crystallization takes place, influence RAF development: the higher the time allowed for the arrangement of the polymer segments into ordered structure, the smaller the layer of immobilized amorphous segments around the crystals.

Isothermal Crystallizations and Successive Melting. Isothermal crystallizations at sufficiently low and comparable rate can emphasize the role of the crystallization temperature on the rigid amorphous fraction development. In this regard, PHB was isothermally crystallized at different temperatures, specifically between 40 and 110 °C, i.e., above and below the critical temperature of 70 °C, and the successive melting behavior was monitored in dependence on T_c.

The time evolution of the crystalline weight fraction (w_C), calculated dividing the integrated area of the exothermal signals by $\Delta h_m°(T)$ at the respective T_c's, is illustrated in Figure 6. An isotherm of 40 min is sufficiently long to guarantee completion of the phase transition at all the investigated T_c's. The maximum of the crystallization rate was found to occur around 70−80 °C, in agreement with literature data.[46] With increasing T_c, the final crystalline weight fraction ($w_C°$) increases progressively, as also shown in inset of Figure 6, where the $w_C°$ data are reported as a function of T_c. Two straight lines with different slope intersecting at T_c = 70 °C suggest that a change in the crystal formation/reorganization mechanism occurs approximately around this temperature.

With changing the crystallization temperature, some variations in the successive melting behavior can also be observed, as exampled in Figure 7, which presents the specific heat capacity (c_p) of PHB recorded at 10 °C min^{-1} immediately after 40 min of isothermal crystallization at the various T_c's. Multiple thermal events can be observed in the c_p curves gained after crystallization at temperatures lower than 70 °C (Figure 7B). After a small endotherm in the c_p plot, which can be

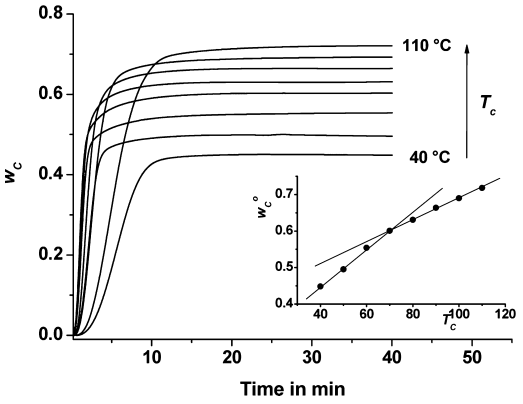

Figure 6. Time evolution of crystalline weight fractions (w_C) of PHB during isothermal crystallization at T_c = 40 °C, 50 °C, 60 °C, 70 °C, 80 °C, 90 °C, 100 °C, 110 °C. In the inset the final crystalline weight fraction ($w_C°$) is depicted as a function of T_c.

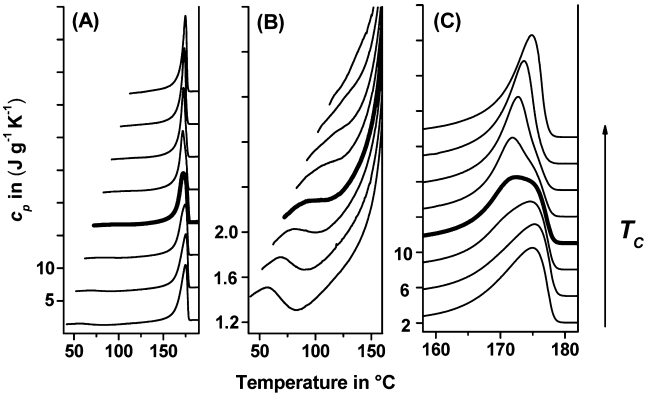

Figure 7. (A) Specific heat capacity (c_p) of PHB upon heating at 10 °C min^{-1} after isothermal crystallization for 40 min at T_c = 40 °C, 50 °C, 60 °C, 70 °C, 80 °C, 90 °C, 100 °C, 110 °C. B and C are enlargements of A. The thick solid line is the c_p curve after crystallization at T_c = 70 °C. The ordinate values refer only to the bottom curve (T_c = 40 °C). All the other curves are shifted vertically for the sake of clearness.

connected to initial partial melting and/or enthalpy recovery subsequent to structural relaxation of the RAF that mobilizes simultaneously with the fusion of smaller or less perfect crystals,[13,32] the DSC curves display an exotherm that extends up to to 120 °C. This exothermic event is not observed after crystallization at T_c > 70 °C, which suggests that crystallization occurring at T_c < 70 °C may be interrupted at a certain stage. Such trend can be rationalized by considering that PHB crystallization at temperatures lower than 70 °C is accompanied by partial vitrification of amorphous chain portions, which creates an immobilized layer around the crystals that hinders further crystallization.[32] Mobilization of this rigid amorphous layer, which could be almost completed around 70 °C, can improve and increase the mobility of the amorphous segments coupled with the crystal, permitting the chain rearrangement needed to form ordered structure, and as a consequence, promoting further crystallization and/or recrystallization. Crystallization conducted at temperatures higher than 70 °C, as a consequence of the higher mobility of the polymer segments, should take place without development of rigid amorphous fraction and therefore be completed in one single stage.

dx.doi.org/10.1021/jp4063127 | J. Phys. Chem. B 2013, 117, 12303−12311

Also the enlargement of the c_p curves in the region of the main melting peak (Figure 7C) confirms the discontinuity in the thermal behavior observed after crystallization at temperatures lower and higher than 70 °C, respectively. PHB samples crystallized below 70 °C present a single broad melting peak, whose maximum is located at about 176 °C. With increasing the crystallization temperature, a second endotherm emerges at slightly lower temperatures, around 173 °C. After crystallization at 70 °C, the overall melting peak results from the superposition of two endotherms with comparable intensity. After crystallization at T_c > 70 °C, the peak at 173 °C becomes predominant, whereas the one centered at 176 °C progressively disappears with the increase in T_c. The establishment of a rigid amorphous layer coupled with the crystals at T_c < 70 °C can explain the different melting behavior. During the heating scan that follows isothermal crystallization, the rigid amorphous fraction devitrifies, and the enhanced mobility of the amorphous chains in contact with the crystals promotes the reorganization/recrystallization processes. The resulting reorganized crystals have higher thermal stability and undergo fusion at somewhat higher temperatures. Conversely, after crystallization at T_c > 70 °C, the positive action exerted by the RAF mobilization onto the reorganization/recrystallization of the original crystals can be missing, which could result in a slightly lower melting temperature. With increasing T_c above 80 °C, more and more perfect crystals grow, as evidenced by the melting peak that becomes narrower and shifts progressively to higher temperature, which indicates that a more uniform population of crystals develops with increasing T_c.

In order to promote crystal reorganization processes during heating and emphasize their effects, heating scans at a lower rate, 5 °C min^{-1}, were also performed immediately after PHB crystallization, starting from the respective T_c's. The DSC curves upon heating at 5 °C min^{-1}, illustrated in Figure 8, show

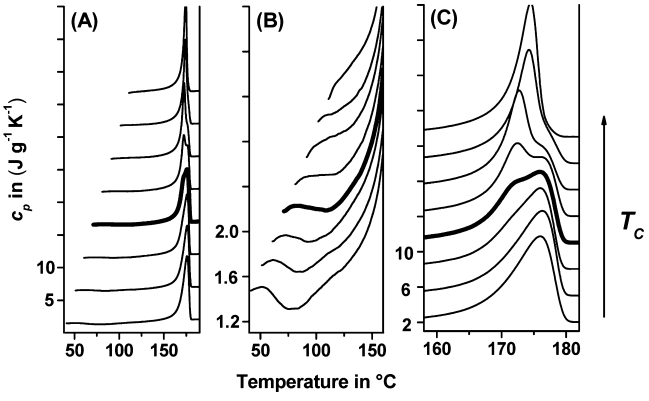

Figure 8. (A) Specific heat capacity (c_p) of PHB upon heating at 5 °C min^{-1} after isothermal crystallization for 40 min at T_c = 40 °C, 50 °C, 60 °C, 70 °C, 80 °C, 90 °C, 100 °C, 110 °C. B and C are enlargements of A. The thick solid line is the c_p curve after crystallization at T_c = 70 °C. The ordinate values refer only to the bottom curve (T_c = 40 °C). All the other curves are shifted vertically for the sake of clarity.

that the overall melting behavior at 5 °C min^{-1} is very similar to that observed at 10 °C min^{-1}; the only notable difference is that a crystallization/recrystallization event of small intensity is also observed after crystallization at 70 °C (Figure 8B). It is likely that during isothermal crystallization at this temperature, a small amount of RAF develops. After crystallization at 80 °C and at higher temperatures, this exothermic event is not observed, as shown in Figure 8B. Also the enlargement of the c_p curves in the region of the main melting peak, presented in Figure 8C, evidence the more intense reorganization that occurs during the scan at 5 °C min^{-1}: the peak at higher temperature, which results from crystal reorganization, remains predominant up to T_c = 70 °C, then progressively reduces, as also seen in Figure 7.

Quasi-isothermal TMDSC Crystallizations and Successive Melting. With the aim of further highlight how the crystallization temperature influences the RAF development, quasi-isothermal crystallization of PHB was performed at 30 °C, i.e., below the discontinuity temperature of 70 °C. Crystallization was conducted in quasi-isothermal mode, in order to simultaneously monitor the evolution of the crystal and of the two amorphous fractions during crystallization.[10]

The time evolution of the reversing specific heat capacity during quasi-isothermal melt crystallization at 30 °C at two different modulation periods (p = 60 and 120 s) is presented in the inset of Figure 9. The two $c_{p,rev}$ curves perfectly overlap,

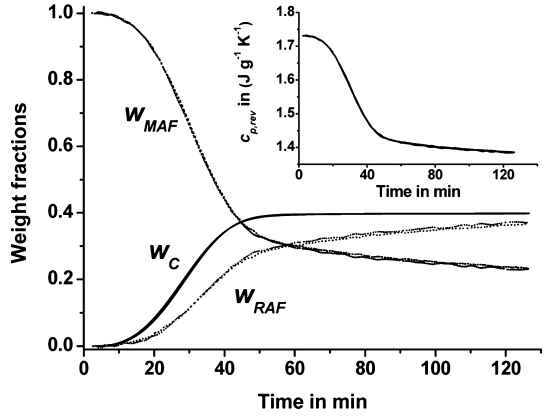

Figure 9. Time evolution of crystalline (w_C, solid lines), mobile amorphous (w_{MAF}, dashed lines) and rigid amorphous (w_{RAF}, dotted lines) weight fractions of PHB during quasi-isothermal crystallization at T_c = 30 °C (p = 60 s and 120 s, A_T = 1.0 °C). The inset shows the time evolution of the reversing specific heat capacities ($c_{p,rev}$) with A_T = 1.0 °C and p = 60 s and 120 s, respectively. Note that both the two curves are depicted.

which ensures that the reversing specific heat capacity truly corresponds to the baseline heat capacity during crystallization at 30 °C. The reversing specific heat capacity decays with time from the liquid c_p at 30 °C: a more marked reduction is noted between 20 and 50 min, then the decrease in $c_{p,rev}$ becomes much slower. According to eq 6, the time evolution of the mobile amorphous fraction at 30 °C was determined from the $c_{p,rev}$ curve, whereas the growth kinetics of the crystalline fraction was derived from the partial areas of the average exothermal signal divided by $\Delta h_m°(T)$ at 30 °C. RAF evolution was determined by difference, as detailed above.

Results of the quasi-isothermal analysis are illustrated in Figure 9. The crystal fraction seems to level off at a constant value, whereas w_{MAF} and w_{RAF} are found to decrease and increase, respectively, even if at slower rate after 50 min from the beginning of the crystallization. Actually, w_C also continues to slightly increase with time (between 50 and 120 min, w_C increases about 0.05), which reveals that at low T_c and long crystallization time, the crystallization of very small amount of material, occurring in geometrically restricted areas, induces the stiffening of considerable amorphous regions in PHB.[27] w_C and

dx.doi.org/10.1021/jp4063127 | J. Phys. Chem. B 2013, 117, 12303−12311

w_{RAF} attained after 120 min of quasi-isothermal modulation around 30 °C are 0.40 and 0.37, respectively. Figure 9 also displays that during isothermal crystallization at 30 °C, the rigid amorphous fraction develops in parallel with the crystals from the beginning of the phase transition. Comparison with the different RAF development attained during nonisothermal crystallization at −2 °C min^{-1}, where PHB crystals mostly grow at higher temperatures and the RAF starts to develop only during the final stages of the crystallization process, allows one to prove that RAF vitrification during crystallization depends on T_c. At low temperatures (below 70 °C), the organization of the polymeric segments into ordered crystal structures is hindered by the limited chain mobility, which leads to large coupling between crystalline and amorphous areas, with high stress transmitted to the amorphous segments, and a high number of chain segments subjected to geometrical limitations. Conversely, at high crystallization temperatures the enhanced chain mobility does not favor the immobilization of amorphous segments, which occurs only when topological restrictions in geometrically limited areas inhibit motions and organization of the polymeric segments.

Figure 10 shows the specific heat capacity (c_p) of PHB recorded upon heating after quasi-isothermal crystallization at

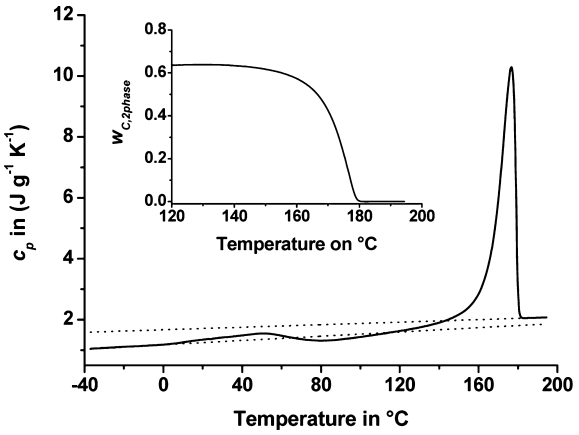

Figure 10. Specific heat capacity of PHB upon heating at 10 °C min^{-1} after quasi-isothermal crystallization at T_c = 30 °C. The black thin dotted lines are the solid and liquid PHB specific heat capacities.[9] In the inset, the crystalline weight fraction, calculated according to the two-phase method by eq 2, is reported.

30 °C. After a first small endotherm, centered at about 50 °C, which can be connected to initial melting and/or enthalpy recovery subsequent to structural relaxation of the RAF,[13,32] a wide exotherm extending approximately from 70 °C up to 120 °C is very evident. The crystalline weight fraction, calculated at temperatures higher than 120 °C by eq 2 according to the two-phase method, reveals that the cold crystallization produces a marked increase in crystallinity, which changes from 0.40, at the end of the quasi-isothermal crystallization, to 0.64. This result confirms that the RAF mobilization, which is complete at about 70 °C, favors the chain rearrangement needed to form ordered structure and permits further crystallization.

CONCLUSIONS

Nonisothermal and quasi-isothermal TMDSC analyses revealed that the evolution of the crystalline, mobile amorphous, and rigid amorphous fractions of PHB depends on the temperature range at which crystallization occurs.

The rigid amorphous fraction grows in parallel with crystalline phase from the beginning of the process during quasi-isothermal crystallization at 30 °C, whereas during nonisothermal crystallization at −2 °C min^{-1}, RAF starts to develop at 70 °C, in correspondence with the final stages of the crystallization process. The RAF achieved after nonisothermal crystallization at 30 °C is much higher than that grown during nonisothermal crystallization at −2 °C min^{-1}, whose peak is centered at about 108 °C. Amorphous segments, which remain mobile at the end of crystallization, can vitrify upon further cooling, because internal stresses, established during crystal growth and concentrated at the interface between the crystal and amorphous phases, can cause immobilization of other segments when the temperature, and therefore the chain mobility is reduced. Analysis of the melting behavior after cooling at −2 °C min^{-1} reveals that RAF devitrification parallels the RAF development: upon heating, the RAF mobilizes at the same temperature at which it had previously grown during the solidification process. Complete RAF mobilization is achieved at about 70 °C.

These results prove that RAF vitrification depends on the mobility of the chains, which in turn is closely connected to the temperature: a lower chain mobility implies a more difficult organization of the entangled chain segments in ordered crystal structures, so that a larger rigid amorphous fraction develops also during the first stages of crystallization. Conversely, at high crystallization temperature, due to the high chain mobility, RAF vitrification occurs only when topological constraints in geometrically restricted areas inhibit motions and organization of the polymeric segments.

The results of the nonisothermal and quasi-isothermal crystallizations together with the analysis of the melting behavior after isothermal crystallizations at various T_c's seem to indicate that 70 °C is the critical temperature for the formation and disappearance of rigid amorphous phase in the PHB sample analyzed in the present study.

In order to complete the picture of the development of the nanophase structure of PHB, the influence of molecular mass on the critical temperature for the formation and disappearance of the rigid amorphous fraction will be investigated in a forthcoming study.

AUTHOR INFORMATION

Corresponding Author

*E-mail: cristina.righetti@ipcf.cnr.it; phone: +39 050 3152068; fax: +39 050 3152230.

Notes

The authors declare no competing financial interest.

REFERENCES

(1) Wunderlich, B. *Thermal Analysis of Polymeric Materials*; Springer-Verlag: New York, 2005.

(2) Wunderlich, B. Reversible Crystallization and the Rigid Amorphous Phase in Semicrystalline Macromolecules. *Prog. Polym. Sci.* **2003**, *28*, 383−450.

(3) Androsch, R.; Wunderlich, B. The Link between Rigid Amorphous Fraction and Crystal Perfection in Cold-Crystallized Poly(ethylene terephthalate). *Polymer* **2005**, *46*, 12556−12566.

(4) Xu, X.; Ince, S.; Cebe, P. Development of the Crystallinity and Rigid Amorphous Fraction in Cold-Crystallized Isotactic Polystyrene. *J. Polym. Sci., Part B: Polym. Phys.* **2003**, *41*, 3026−3036.

(5) Xu, H.; Cebe, P. Heat Capacity Study of Isotactic Polystyrene: Dual Reversing Crystal Melting and Relaxation of Rigid Amorphous Fraction. *Macromolecules* **2004**, *37*, 2797−2806.

(6) Righetti, M. C.; Tombari, E.; Angiuli, M.; Di Lorenzo, M. L. Enthalpy-Based Determination of Crystalline, Mobile Amorphous and Rigid Amorphous Fractions in Semicrystalline Polymers: Poly(ethylene terephthalate). *Thermochim. Acta* **2007**, *462*, 15−24.
(7) Righetti, M. C.; Tombari, E.; Di Lorenzo, M. L. Crystalline, Mobile Amorphous and Rigid Amorphous Fractions in Isotactic Polystyrene. *Eur. Polym. J.* **2008**, *44*, 2659−26676.
(8) Chen, H.; Cebe, P. Vitrification and Devitrification of Rigid Amorphous Fraction of PET during Quasi-Isothermal Cooling and Heating. *Macromolecules* **2009**, *42*, 288−292.
(9) Schick, C.; Wurm, A.; Mohamed, A. Vitrification and Devitrification of the Rigid Amorphous Fraction of Semicrystalline Polymers Revealed from Frequency-Dependent Heat Capacity. *Colloid Polym. Sci.* **2001**, *279*, 800−806.
(10) Schick, C.; Wurm, A.; Mohammed, A. Formation and Disappearance of the Rigid Amorphous Fraction in Semicrystalline Polymers Revealed from Frequency Dependent Heat Capacity. *Thermochim. Acta* **2003**, *396*, 119−132.
(11) Righetti, M. C.; Tombari, E. Crystalline, Mobile Amorphous and Rigid Amorphous Fractions in Poly(L-lactic acid) by TMDSC. *Thermochim. Acta* **2011**, *522*, 118−127.
(12) Minakov, A. A.; Mordvintsev, D. A.; Tol, R.; Schick, C. Melting and Reorganization of the Crystalline Fraction and Relaxation of the Rigid Amorphous Fraction of Isotactic Polystyrene on Fast Heating (30,000 K/min). *Thermochim. Acta* **2006**, *442*, 25−30.
(13) Righetti, M. C.; Di Lorenzo, M. L.; Tombari, E.; Angiuli, M. The Low-Temperature Endotherm in Poly(ethylene terephthalate): Partial Melting and Rigid Amorphous Fraction Mobilization. *J. Phys. Chem. B* **2008**, *112*, 4233−4241.
(14) Di Lorenzo, M. L. The Melting Process and the Rigid Amorphous Fraction in *cis*-1,4-Polybutadiene. *Polymer* **2009**, *50*, 578−584.
(15) Righetti, M. C.; Di Lorenzo, M. L.; Angiuli, M.; Tombari, E. Structural Reorganization in Poly(butylene terephthalate) during Fusion. *Macromolecules* **2004**, *37*, 9027−9033.
(16) Di Lorenzo, M. L.; Righetti, M. C.; Cocca, M.; Wunderlich, B. Coupling between Crystal Melting and Rigid Amorphous Fraction Mobilization in Poly(ethylene terephthalate). *Macromolecules* **2010**, *43*, 7689−7694.
(17) Di Lorenzo, M. L.; Righetti, M. C. The Three-Phase Structure of Isotactic Poly(1-butene). *Polymer* **2008**, *49*, 1323−1331.
(18) Di Lorenzo, M. L.; Righetti, M. C.; Wunderlich, B. Influence of Crystal Polymorphism on the Three-Phase Structure and on the Thermal Properties of Isotactic Poly(1-butene). *Macromolecules* **2009**, *42*, 9312−9320.
(19) Martin, S.; Exposito, M. T.; Vega, J. F.; Martinez-Salazar, J. Microstructure and Properties of Branched Polyethylene: Application of a Three-Phase Structural Model. *J. Appl. Polym. Sci.* **2013**, *128*, 1871−1878.
(20) Lin, J.; Shenogin, S.; Nazarenko, S. Oxygen Solubility and Specific Volume of Rigid Amorphous Fraction in Semicrystalline Poly(ethylene terephthalate). *Polymer* **2002**, *43*, 4733−4743.
(21) Guinault, A.; Sollogoub, C.; Ducruet, V.; Domenek, S. Impact of Crystallinity of Poly(lactide) on Helium and Oxygen Barrier Properties. *Eur. Polym. J.* **2012**, *48*, 779−788.
(22) Kolesov, I.; Androsch, R. The Rigid Amorphous Fraction of Cold-Crystallized Polyamide 6. *Polymer* **2012**, *53*, 4770−4777.
(23) Delpouve, N.; Stoclet, G.; Saiter, A.; Dargent, E.; Marais, S. Water Barrier Properties in Biaxially drawn Poly(lactic acid) Films. *J. Phys. Chem. B* **2012**, *116*, 4615−4625.
(24) Sudesh, K.; Abe, H.; Doi, Y. Synthesis, Structure and Properties of Polyhydroxyalkanoates: Biological Polyesters. *Prog. Polym. Sci.* **2000**, *25*, 1503−1555.
(25) Ha, C.-S.; Cho, W.-J. Miscibility, Properties, and Biodegradability of Microbial Polyester Containing Blends. *Prog. Polym. Sci.* **2002**, *27*, 759−809.
(26) Androsch, R. Surface Structure of Folded-chain Crystals of Poly(*R*-3-hydroxybutyrate) of Different Chain Length. *Polymer* **2008**, *49*, 4673−4679.
(27) Di Lorenzo, M. L.; Righetti, M. C. Effect of Thermal History on the Evolution of Crystal and Amorphous Fractions of Poly[(R)-3-hydroxybutyrate] upon Storage at Ambient Temperature. *Eur. Polym. J.* **2012**, *49*, 510−517.
(28) Di Lorenzo, M. L.; Righetti, M. C. Evolution of Crystal and Amorphous Fractions of Poly[(*R*)-3-hydroxybutyrate] upon Storage. *Therm. Anal. Calorim.* **2013**, *112*, 1439−1446.
(29) El-Taweel, S. H.; Höhne, G. W. H.; Mansour, A. A.; Stoll, B.; Selinger, H. Glass Transition and the Rigid Amorphous Phase in Semicrystalline Blends of Bacterial Polyhydroxybutyrate PHB with Low Molecular Mass Atactic *R*,*S*-PHB-diol. *Polymer* **2004**, *45*, 983−992.
(30) Androsch, R. Melt-Crystallization, Glass Transition and Morphology of a (*R*)-3-Hydroxybutyrate Pentamer. *Eur. Polym. J.* **2007**, *43*, 93−108.
(31) Androsch, R. Melt-Crystallization, Glass Transition and Morphology of (R)-3-Hydroxybutyrate Oligomers. *Eur. Polym. J.* **2007**, *43*, 4961−4974.
(32) Di Lorenzo, M. L.; Gazzano, M.; Righetti, M. C. The Role of the Rigid Amorphous Fraction on Cold Crystallization of Poly(3-hydroxybutyrate). *Macromolecules* **2012**, *45*, 5684−5691.
(33) Sarge, S. M.; Hemminger, W.; Gmelin, E.; Höhne, G. W. H.; Cammenga, H. K.; Eysel, W. Metrologically Bases Procedures for the Temperature, Heat and Heat Flow Rate Calibration of DSC. *J. Therm. Anal.* **1997**, *49*, 1125−1134.
(34) Di Lorenzo, M. L.; Sajkiewicz, P.; La Pietra, P.; Gradys, A. Irregularly Shaped DSC Exotherms in the Analysis of Polymer Crystallization. *Polym. Bull.* **2006**, *57*, 713−721.
(35) Di Lorenzo, M. L.; Sajkiewicz, P.; Gradys, A. Optimization of the Melting Conditions for the Analysis of Crystallization Kinetics of Poly(3-hydroxybutyrate). *e-Polym.* **2009**, n.27.
(36) Wunderlich, B. Modeling the Heat Flow and Heat Capacity of Modulated Differential Scanning Calorimetry. *J. Therm. Anal.* **1997**, *48*, 207−224.
(37) Wurm, A.; Merzlyakov, M.; Schick, C. Reversible Melting Probed by Temperature Modulated Dynamic Mechanical and Calorimetric Measurements. *Colloid Polym. Sci.* **1998**, *276*, 289−296.
(38) Androsch, R.; Moon, I.; Kreitmeier, S.; Wunderlich, B. Determination of Heat Capacity with a Sawtooth-Type, Power Compensated Temperature Modulated DSC. *Thermochim. Acta* **2000**, *357*−*358*, 267−278.
(39) Di Lorenzo, M. L.; Wunderlich, B. Melting of Polymers by Non-Isothermal, Temperature-Modulated Calorimetry: Analysis of Various Irreversible Latent Heat Contributions to the Reversing Heat Capacity. *Thermochim. Acta* **2003**, *405*, 255−268.
(40) Di Lorenzo, M. L.; Wunderlich, B. Temperature-Modulated Calorimetry of the Crystallization of Polymers Analyzed by Measurements and Model Calculations. *J. Therm. Anal. Calorim.* **1999**, *57*, 459−472.
(41) Merzlyakov, M.; Schick, C. Complex Heat Capacity Measurements by TMDSC Part 1. Influence of Non-linear Thermal Response. *Thermochim. Acta* **1999**, *330*, 55−64.
(42) Merzlyakov, M.; Schick, C. Optimization of Experimental Parameters in TMDSC. The Influence of Non-linear and Non-stationary Thermal Response. *J. Therm. Anal. Calorim.* **2000**, *61*, 649−659.
(43) Schick, C.; Wurm, A.; Mohammed, A. Dynamics of Reversible Melting Revealed from Frequency Dependent Heat Capacity. *Thermochim. Acta* **2002**, *392*−*393*, 303−313.
(44) Mathot, V. B. F. *Calorimetry and Thermal Analysis of Polymers*; Hanser Verlag: Munich, Germany, 1994.
(45) Ma, Q.; Georgiev, G.; Cebe, P. Constraints in Semicrystalline Polymers: Using Quasi-Isothermal Analysis to Investigate the Mechanism of Formation and Loss of the Rigid Amorphous Fraction. *Polymer* **2011**, *52*, 4562−4570.
(46) Pizzoli, M.; Scandola, M.; Ceccorulli, G. Crystallization and Melting of Isotactic Poly(3-hydroxy butyrate) in the Presence of a Low Molecular Weight Diluent. *Macromolecules* **2002**, *35*, 3937−3941.